

# Structure and Dynamics of Multiple Cationic Vectors–siRNA Complexation by All-Atomic Molecular Dynamics Simulations

Defang Ouyang,<sup>†,‡</sup> Hong Zhang,<sup>‡</sup> Harendra S. Parekh,<sup>\*,†</sup> and Sean C. Smith<sup>\*,‡</sup>

School of Pharmacy and Centre for Computational Molecular Science, Australian Institute of Bioengineering and Nanotechnology, The University of Queensland, Brisbane, QLD 4072, Australia

Received: December 17, 2009; Revised Manuscript Received: June 1, 2010

Understanding the molecular mechanism of gene condensation is a key component to rationalizing gene delivery phenomena, including functional properties such as the stability of the gene–vector complex and the intracellular release of the gene. In this work, we adopt an atomistic molecular dynamics simulation approach to study the complexation of short strand duplex RNA with four cationic carrier systems of varying charge and surface topology at different charge ratios. At lower charge ratios, polymers bind quite effectively to siRNA, while at high charge ratios, the complexes are saturated and there are free polymers that are unable to associate with RNA. We also observed reduced fluctuations in RNA structures when complexed with multiple polymers in solution as compared to both free siRNA in water and the single polymer complexes. These novel simulations provide a much better understanding of key mechanistic aspects of gene–polycation complexation and thereby advance progress toward rational design of nonviral gene delivery systems.

## 1. Introduction

Gene condensation—the first and key step toward successful nonviral gene delivery—is highly dependent upon the stability of complexation with vector particles. This stability also intrinsically affects the intracellular release of genes from their vectors, a factor that ultimately determines transfection rates in vitro and in vivo.<sup>1</sup> There are many aspects of gene–vector complexation that need to be considered, including—but not limited to—carrier type and morphology, molecular weight, nitrogen (vector) to phosphate (gene) (N/P) charge ratios, salt concentration, and the type/size of gene.<sup>1–3</sup> Various techniques have been employed to assist in determining optimal parameters for gene–vector complexation including atomic force microscopy and dynamic light scattering.<sup>4</sup> In one such study investigating poly(2-dimethylaminoethylmethacrylate) homopolymer/DNA complexation at a 1/1 polymer–DNA weight ratio, poorly condensed structures were observed, while complexes at 2/1 polymer–DNA weight ratio resulted in more tight clusters. Another study reported similar findings, although agarose gel electrophoresis (GE) was employed.<sup>5</sup> Here, poly(L-lysine) (PLL)–DNA complexes at N/P ratios >1.0 were fully retained in the well (i.e., completely retarded DNA migration indicating effective complexation by PLL), while complexes at N/P ratios <1 saw partial DNA migration across the gel. Ethidium bromide displacement assays are considered another reliable indicator of effective gene–vector complexation, having been found to be in general agreement with GE. The ability to monitor the intracellular trafficking and fate of complexes at the single-cell level represents a model scenario, having been achieved with some success using fluorescence correlation spectroscopy.<sup>6</sup> Researchers have been able to investigate the formation and dissociation of complexes, this adding an extra dimension and

allowing (with the appropriate labeling) tracking of complexes and their respective component parts in live cells.

Many reports to date rely on in vitro studies being performed in an iterative manner, in the hope that desired outcomes for the gene (high transfection rates) and vector (low toxicity) being delivered will eventually be attained. There exists limited focus on the in silico rational design of vectors, namely, due to experimental complexities and lengthy computing times required to complete simulations.<sup>7–13</sup> Recently, molecular dynamics (MD) simulation has been identified as a powerful tool in helping to answer many fundamental questions that gene delivery scientists inadvertently overlook but rely on for success in gene delivery studies in vitro/in vivo. MD simulation offers a unique insight into the energetic effects of binding between (dendritic) molecules and DNA, providing crucial data on the association and dissociation potential of vector and gene.<sup>14</sup> MD simulation generates data that when performed using lifelike models of vector, gene, and the environment offers unique insights into the architecture of complexes, their (in)flexible nature, and final overall charge, all of which contribute in an additive manner to their observed efficacy.<sup>15</sup> Interestingly, to date, very simplistic models of MD simulation in nonviral gene delivery have been reported, and most have employed simple bead models of vectors and genes, a far cry from their actual conformation, thereby limiting the precision of any generated data.

Biological experiments commonly exploit differing charge ratios between the carrier and the gene. Increasing the ± charge ratio, that is, the number of positive charges associated with the vector particles relative to the intrinsic negative charge of the gene, is generally considered to have a beneficial effect in enhancing delivery (although pushing this ratio too far can cause toxicity effects). This is achieved in two ways, either by increasing the size of the cationic vector, such that a single carrier particle carries many more cationic ligand groups, or by increasing the concentration of cationic carrier particles of fixed size relative to that of the gene. In the spirit of working toward a rational design strategy for cationic vectors from the bottom

\* To whom correspondence should be addressed. (H.S.P.) Tel: +61-7-3365 7430. Fax: +61-7-3365 1688. E-mail: h.parekh@pharmacy.uq.edu.au. (S.C.S.) Tel: +61-7-3346 3949. Fax: +61-7-3346-3992. E-mail: s.smith@uq.edu.au.

<sup>†</sup> School of Pharmacy.

<sup>‡</sup> Australian Institute of Bioengineering and Nanotechnology.

**TABLE 1:** Simulated Cell Compositions and Atom Numbers for Multiple Cationic Polymers–siRNA Complexation Systems

	charge ratio	molecule number ratio	atom number of RNA	atom number of polymers	number of counterions	molecule number of water	total atom number
4 <sup>+</sup> linearlysine	0.6/1	6/1	1335	624	16 Na <sup>+</sup>	17444	54307
	1/1	10/1	1335	1040	0	17298	54269
	2/1	20/1	1335	2080	40 Cl <sup>-</sup>	38091	117727
4 <sup>+</sup> G0	0.6/1	6/1	1335	528	15 Na <sup>+</sup>	10297	32769
	1/1	10/1	1335	880	0	17519	54772
	2/1	20/1	1335	1760	40 Cl <sup>-</sup>	45622	140001
8 <sup>+</sup> linearlysine	0.6/1	3/1	1335	576	16 Na <sup>+</sup>	26309	80854
	1/1	5/1	1335	960	0	26892	82971
	2/1	10/1	1335	1920	39 Cl <sup>-</sup>	30532	94890
8 <sup>+</sup> G1	0.6/1	3/1	1335	708	15 Na <sup>+</sup>	10354	33120
	1/1	5/1	1335	1180	0	21089	65782
	2/1	10/1	1335	2360	40 Cl <sup>-</sup>	66535	203340

up, we have chosen to explore in more detail the latter approach, namely, the complexation of multiple small cationic dendrons

with short-strand RNA. We explore via atomistic MD simulations the complexation between a 21 base pair duplex small

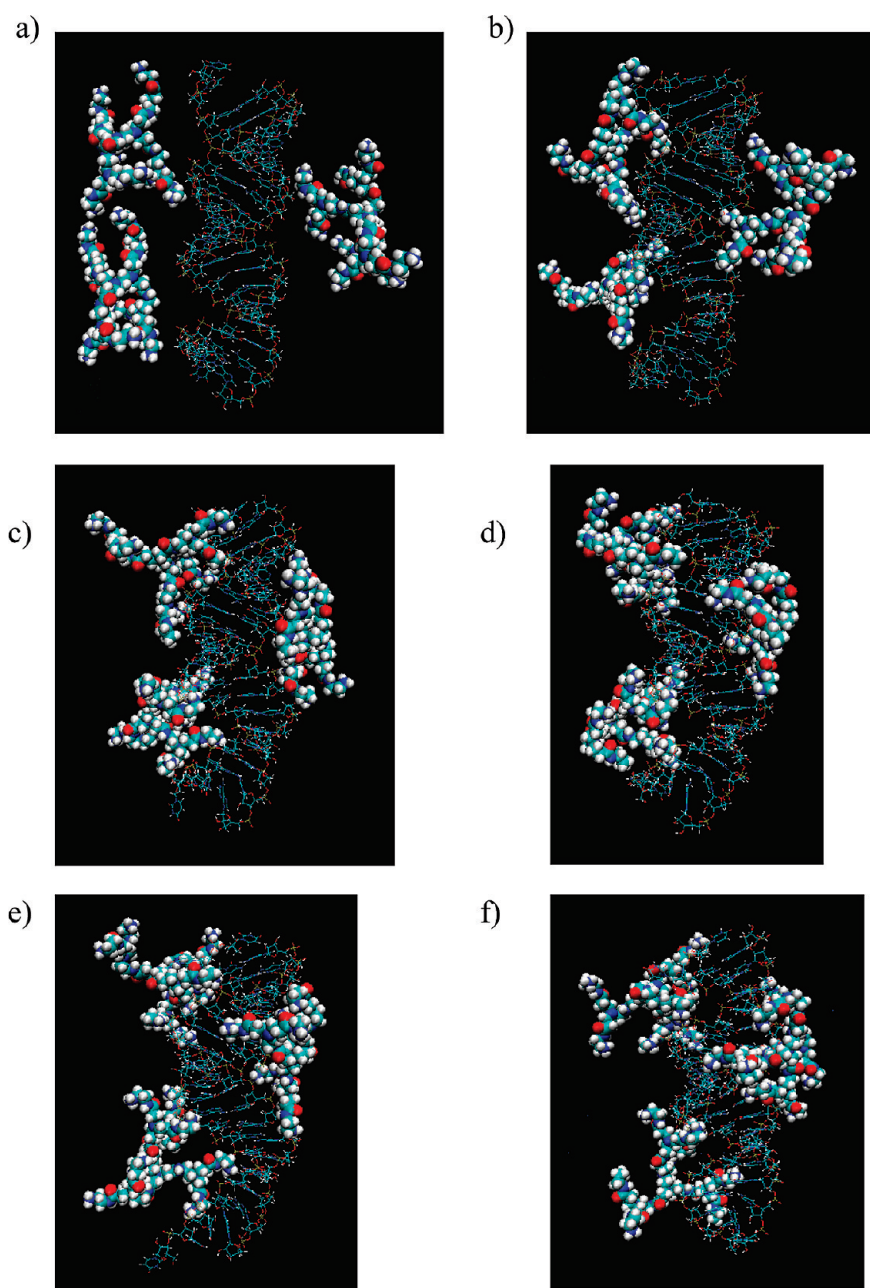


**Figure 1.** Snapshots of 8<sup>+</sup>G1–siRNA complex at a charge ratio of 0.6/1: (a) 0, (b) 2, (c) 4, (d) 6, (e) 8, and (f) 10 ns. Water molecules and counterions are omitted for clarity.

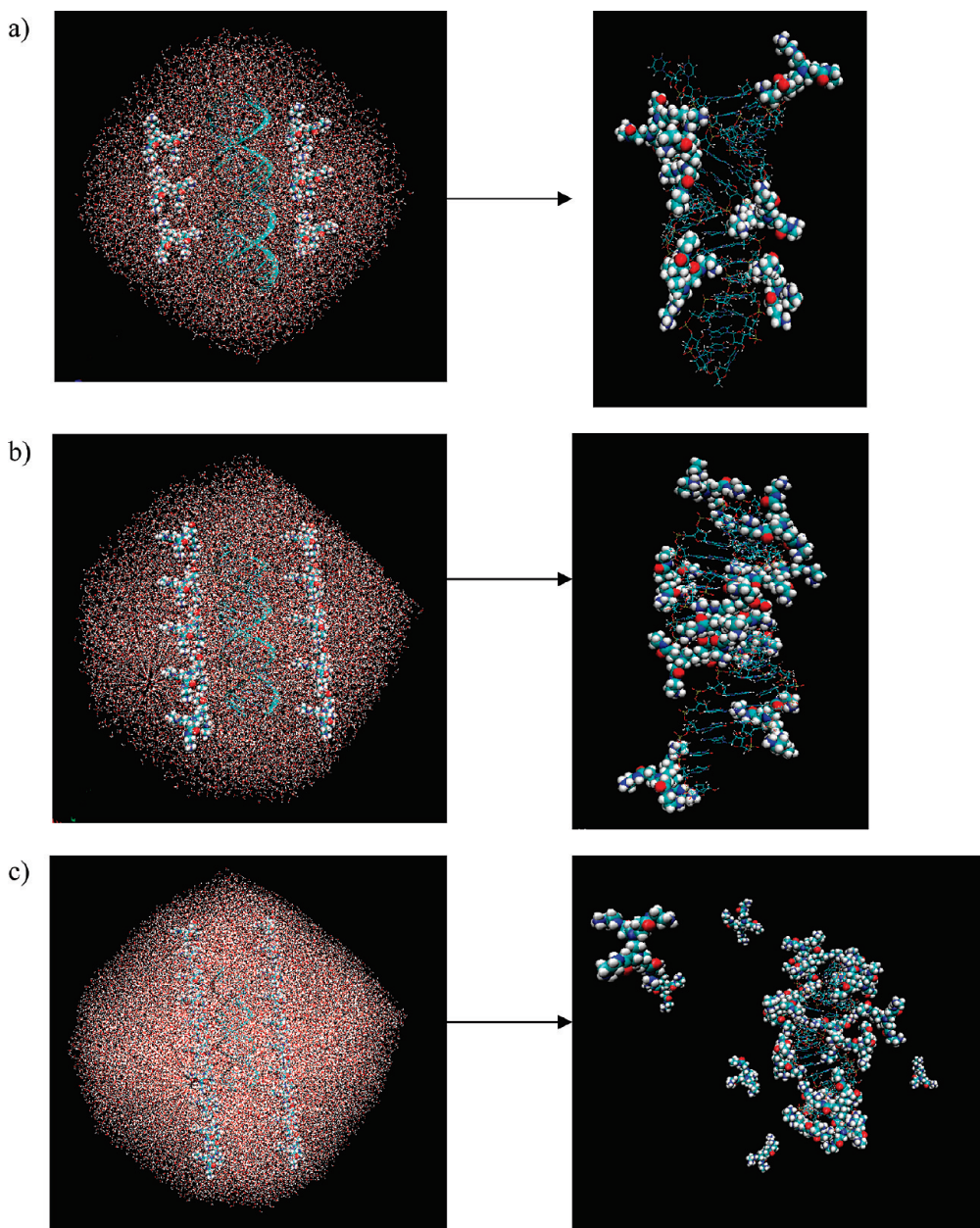


**Figure 2.** Snapshots of  $4^+$ G0–siRNA complex at 0 (left) and 10 ns (right, water molecules and counterions are omitted for clarity): (a) charge ratio of 0.6/1, (b) charge ratio of 1/1, and (c) charge ratio of 2/1.

interfering RNA (siRNA) and four polymers of varying structure at different  $\pm$  charge ratios (0.6/1 and 1/1). Specifically, we study four positive-charged G0-PAMAM dendrimer ( $4^+$ dendrimer), eight positive-charged G1-PAMAM dendrimer ( $8^+$ dendrimer), four positive-charged linear PLL ( $4^+$ linearlysine), and eight positive-charged linear PLL ( $8^+$ linearlysine) (see the Supporting Information, Figure S-1) in explicit water and counterions. All simulations are run by AMBER,<sup>16</sup> and the simulations reveal detailed molecular-level pictures of the structures and dynamics of multiple polycation–RNA complexes.

## 2. Simulation Details

**2.1. MD Simulations.** The sequence of the 21 base pair siRNA is taken from the earlier study by Putral et al.<sup>17</sup> and is as follows:

sense: 5'-GCAACAGUUACUGCGACGUUU-3'

antisense: 3'-UUCGUUGUCAAUGACGCUGCA-5'

The MD simulations utilize the AMBER9 software package<sup>16,18,19</sup> with the all-atom ff99 force field for RNA<sup>20</sup> and the general

AMBER force field (gaff) for all polymers.<sup>21</sup> Duplex RNA was generated by the Nucleic Acid Builder (NAB) (<http://casgroup.rutgers.edu/>). All four polymers were built by Material Studio 4.3 (<http://accelrys.com/products/materials-studio/>), and all of the primary amines were protonated. Using the LEAP module in AMBER 9, the polymers were positioned on both sides of RNA. The electrostatic interactions were calculated with the particle mesh Ewald method,<sup>22–27</sup> and the cutoff was 10 Å. Using the LEAP module in AMBER 9, the complex structure was immersed in a truncated octahedral water box with a solvation shell of 10 Å thickness using the TIP3P model for water.<sup>28</sup> In addition, some water molecules were replaced by  $\text{Na}^+$  counterions to neutralize the negative charge on the phosphate backbone of the RNA structure. The composition of these systems is shown in Table 1.

The minimization procedure for solvated RNA consisted of two steps. In the first stage, the complex was kept fixed, and positions of the water and ions were minimized. The solvated structures were then subjected to 1000 steps of steepest descent

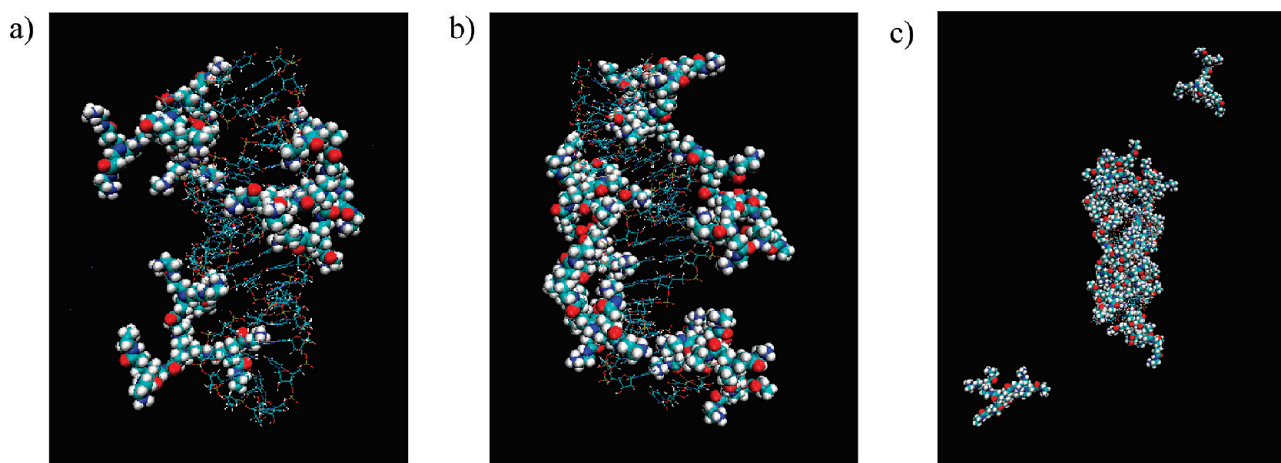


**Figure 3.** Snapshots of  $8^+G1$ –siRNA complex at 10 ns: (a) charge ratio of 0.6/1, (b) charge ratio of 1/1, and (c) charge ratio of 2/1. Water molecules and counterions are omitted for clarity.

**TABLE 2: Number of Polymers Binding siRNA and Amine-Phosphate Contact Points after 10 ns Simulations**

	charge ratio	molecule number	number of binding polymers	number of N–P interactions (within 5 Å)
$4^+G0$	0.6/1	6/1	6	15
	1/1	10/1	9	26
	2/1	20/1	12	32
	0.6/1	6/1	6	15
$8^+G0$	1/1	10/1	10	29
	2/1	20/1	14	34
	0.6/1	3/1	3	19
$8^+linearlysine$	1/1	5/1	5	27
	2/1	10/1	8	36
	0.6/1	3/1	3	17
	8 <sup>+</sup> G1	1/1	5/1	29
	2/1	10/1	8	38

minimization followed by 1000 steps of conjugate gradient minimization.<sup>29,30</sup> During this minimization process, the complex was kept fixed in its starting conformation using harmonic constraints with a force constant of 500 kcal/mol/Å<sup>2</sup>. In the second stage, the entire system was minimized by 2000 steps of steepest descent minimization followed by 8000 steps of conjugate gradient minimization without the restraints.

The minimized structure was then subjected to 20 ps of MD, using a 2 fs time step for integration. During the MD simulation, the system was gradually heated from 0 to 300 K using 10 kcal/mol/Å<sup>2</sup> weak positional restraints on the RNA. The SHAKE

algorithm was used in which all bonds involving hydrogen are constrained.<sup>31</sup> After the system was heated at constant volume with weak restraints on the complex, MD was performed for 10 ns with a time step of 2 fs under constant pressure/constant temperature (NPT ensemble) at 300 K with an average pressure of 1 atm without positional restraints. The random number seed of every restart was changed.<sup>32</sup> Isotropic position scaling<sup>33</sup> was used to maintain the pressure, and a relaxation time of 2 ps was employed. SHAKE was used to constrain bonds involving hydrogen, and the temperature was kept at 300 K with Langevin dynamics<sup>34</sup> using a collision frequency of 1.0 ps<sup>-1</sup>.

### 3. Results and Discussions

**3.1. MD Trajectory Analysis of the RNA–Polymer Complexes.** Snapshots at 2 ns intervals during the 10 ns MD simulations are shown for  $8^+G1$  at charge ratio 0.6/1 in Figure 1. During the simulation, the carriers quickly change their starting position to bind with siRNA within the first 2 ns and then adjust their conformations to reach equilibrium. Figure 2 shows the starting structures and final 10 ns snapshots for simulations at three charge ratios, 0.6/1, 1/1, and 2/1, in which the molecules of  $4^+G0$  are initially positioned equidistant on both sides of siRNA. Figure 3 shows the snapshots of 10 ns for the  $8^+G1$ –RNA simulations at three different charge ratios. Analogous results for  $4^+linearlysine$  and  $8^+linearlysine$  are shown in Figures S-2 and S-3 (see the Supporting Information).

**TABLE 3: Starting Structures and Average Structures of siRNA in 10 ns Simulation for Backbone Angles and Helical Parameters**

starting structures	$4^+G0$			$8^+G1$		
	np0.6/1	np1/1	np2/1	np0.6/1	np1/1	np2/1
x-disp (Å)	$-4.61 \pm 0.28$	$-4.35 \pm 0.72$	$-5.56 \pm 2.56$	$-4.97 \pm 1.47$	$-3.99 \pm 1.00$	$-5.30 \pm 2.62$
y-disp (Å)	$-0.01 \pm 0.05$	$-0.05 \pm 0.27$	$0.06 \pm 1.06$	$-0.54 \pm 2.30$	$0.06 \pm 0.74$	$-0.54 \pm 2.66$
inclination (°)	$16.02 \pm 0.68$	$15.57 \pm 7.36$	$14.79 \pm 8.19$	$20.41 \pm 14.33$	$19.17 \pm 9.49$	$14.14 \pm 11.14$
shift (Å)	$0.00 \pm 0.02$	$0.03 \pm 0.16$	$0.14 \pm 0.45$	$0.12 \pm 0.59$	$0.05 \pm 0.34$	$0.14 \pm 0.62$
slide (Å)	$-1.75 \pm 0.03$	$-1.56 \pm 0.22$	$-1.84 \pm 0.36$	$-1.54 \pm 0.44$	$-1.28 \pm 0.50$	$-1.73 \pm 0.42$
rise (Å)	$3.40 \pm 0.01$	$3.29 \pm 0.14$	$3.35 \pm 0.17$	$3.27 \pm 0.22$	$3.23 \pm 0.30$	$3.34 \pm 0.25$
tilt (°)	$0.00 \pm 0.08$	$0.00 \pm 0.97$	$1.34 \pm 1.47$	$-0.01 \pm 1.65$	$0.71 \pm 3.02$	$0.06 \pm 1.55$
roll (°)	$8.91 \pm 0.12$	$8.36 \pm 4.17$	$6.74 \pm 2.79$	$9.40 \pm 4.40$	$10.33 \pm 5.17$	$6.33 \pm 3.98$
twist (°)	$31.55 \pm 1.23$	$30.09 \pm 1.60$	$27.73 \pm 6.18$	$27.68 \pm 6.15$	$29.83 \pm 3.43$	$27.96 \pm 6.34$
shear (Å)	$0.00 \pm 0.11$	$-0.02 \pm 0.14$	$0.17 \pm 0.82$	$0.01 \pm 0.15$	$0.03 \pm 0.19$	$0.10 \pm 0.47$
stretch (Å)	$-0.12 \pm 0.06$	$-0.11 \pm 0.06$	$-0.15 \pm 0.12$	$-0.11 \pm 0.08$	$-0.09 \pm 0.08$	$-0.13 \pm 0.08$
stagger (Å)	$0.03 \pm 0.00$	$0.00 \pm 0.07$	$-0.11 \pm 0.15$	$-0.02 \pm 0.16$	$-0.08 \pm 0.33$	$-0.07 \pm 0.22$
buckle (°)	$0.00 \pm 0.20$	$-0.74 \pm 4.57$	$-2.63 \pm 6.99$	$0.65 \pm 7.83$	$2.06 \pm 12.24$	$0.69 \pm 7.83$
propelleer (°)	$13.74 \pm 0.01$	$-14.57 \pm 2.41$	$-9.20 \pm 5.01$	$-12.82 \pm 4.70$	$-14.62 \pm 7.87$	$-10.14 \pm 3.47$
opening (°)	$-5.52 \pm 0.13$	$0.55 \pm 1.06$	$-1.22 \pm 2.51$	$1.21 \pm 2.45$	$1.41 \pm 2.34$	$0.58 \pm 2.03$

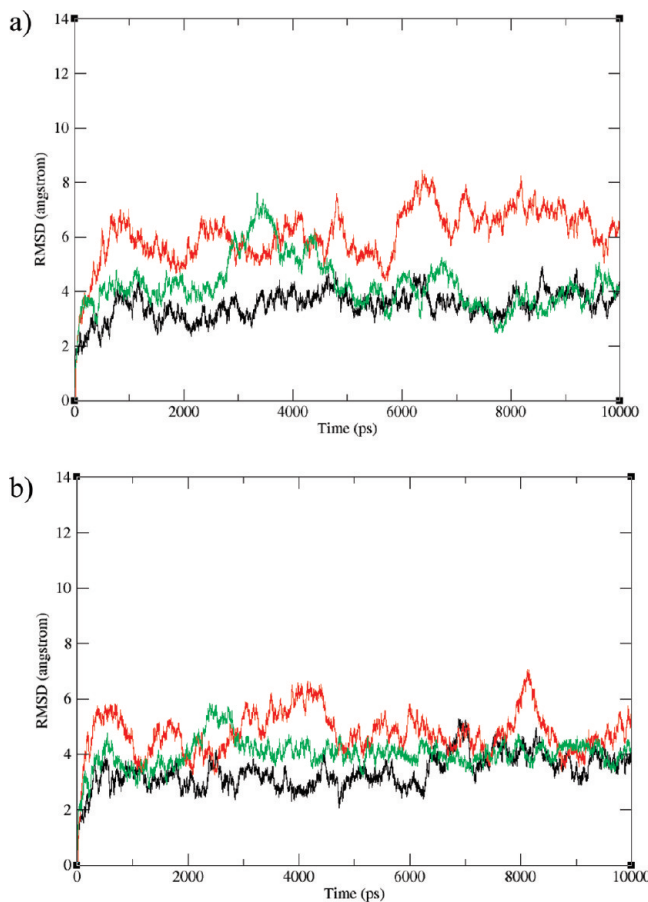


**Figure 4.** rmsd vs time of polymer–RNA complexation in 10 ns: (a) 4<sup>+</sup>G1–RNA complex and (b) 8<sup>+</sup>G1–RNA complex (0.6/1, black; 1/1, red; and 2/1, green).

Three very interesting trends become apparent from these figures. First, while at lower charge ratios, both 4<sup>+</sup>polymer and 8<sup>+</sup>polymer bind quite effectively to siRNA; as the charge ratio increases, it becomes increasingly apparent that the complexes begin to saturate. Polymers are seen to come off into solution for periods before rejoining the complex, such that all of the carriers are not bound to the RNA all of the time. This is in agreement with previous reports, although large numbers of polymers (86%) free of RNA association were detected at higher charge ratios (>6).<sup>6</sup> It is particularly relevant also to note that in the companion paper (DOI: 10.1021/jp911906e), which examines single polymer–RNA complexes, the single 4<sup>+</sup>polymer and 8<sup>+</sup>polymer are never seen to be dissociated from the complex during 18 ns simulations. The probable reason is that the surface area of the RNA is finite; hence, steric crowding becomes a factor with increasing numbers of complexed polymers.

Second, as is apparent in Table 2 from the number of polymer molecules binding and numbers of contact points (of positively charged amine groups with negatively charged phosphate groups), at higher charge ratios, more of the 4<sup>+</sup>polymers become dissociated from the complex at any given time as compared with the 8<sup>+</sup>polymers. Despite this, the actual numbers of contact points remain quite similar. Our results confirmed the previous experimental deduction that only limited neutralization of DNA phosphate groups is required for DNA condensation even at high charge ratios.<sup>6</sup> Two interrelated factors may be identified to rationalize this second trend: (a) As revealed by the binding free energy calculations in the companion paper (DOI: 10.1021/jp911906e), the binding energy for an 8<sup>+</sup>polymer is nearly twice

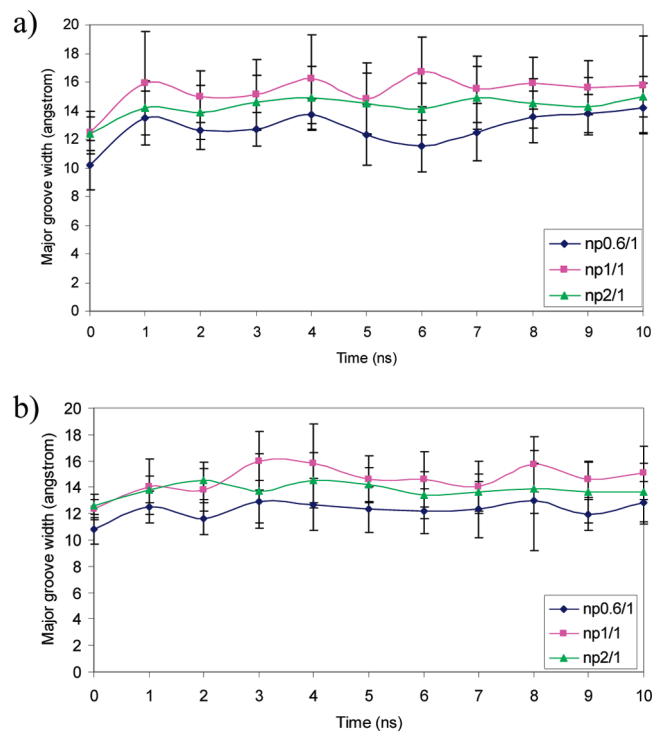


**Figure 5.** Major groove width of siRNA (averaged along the strand) vs time for (a) 4<sup>+</sup>G0 or (b) 8<sup>+</sup>G1–RNA complexation over 10 ns simulations. The major groove width is defined as averaged direct P–P distances of base pairs. The error bars indicate the standard deviation associated with averaging along the length of the strand.

that of a 4<sup>+</sup>polymer and so bind more readily with RNA, and (b) at the same charge ratio, the number of 4<sup>+</sup>polymers is twice that of the 8<sup>+</sup>polymer. Proceeding from these points, one notes that due to the smaller size, the only way for the 4<sup>+</sup>polymer system to relieve steric crowding is for individual dendrimers to come off the complex into solution. On the other hand, the larger 8<sup>+</sup>dendrimers can, to some extent, relieve steric crowding by having some ligands/branches presented externally, while other ligands remain attached to the RNA. Collectively, these considerations provide a suitable explanation for the observed behavior.

The third trend that is apparent from the figures is that there are strong duplex RNA deforming characteristics in the presence of polymer, with the terminal amine group of polymer also making contact with the phosphate groups of the RNA. Table 3 compares the backbone angles and helical parameters between the starting structures of siRNA and averaged structures in 10 ns simulation, and we can see apparent variations.

**3.2. Dynamics of the Complex Formation.** The root-mean-squared deviation (rmsd) plots for multiple polymer–RNA complexes are shown in Figure 4 and represent the fluctuation of the heavy atoms of RNA. It is apparent that this parameter has in all cases ceased to increase systematically by around 4 ns, which is indicative that our complexes are reasonably equilibrated during the time scale of our 10 ns simulations. A comparison with the rmsd plots (Figure 5) for the single dendrimer complexes in the companion paper (DOI: 10.1021/jp911906e) reveals that fluctuations are greater in the present multidendrimer simulations. This is to be expected given the dynamical exchange of dendrimers on and off the complex, which naturally leads to increased structural fluctuations during the simulations. Figure 5 shows the variation in the major groove width (averaged along the strand) as a function of simulation time for the 4<sup>+</sup>G0 and 8<sup>+</sup>G1 complexes. The major groove width

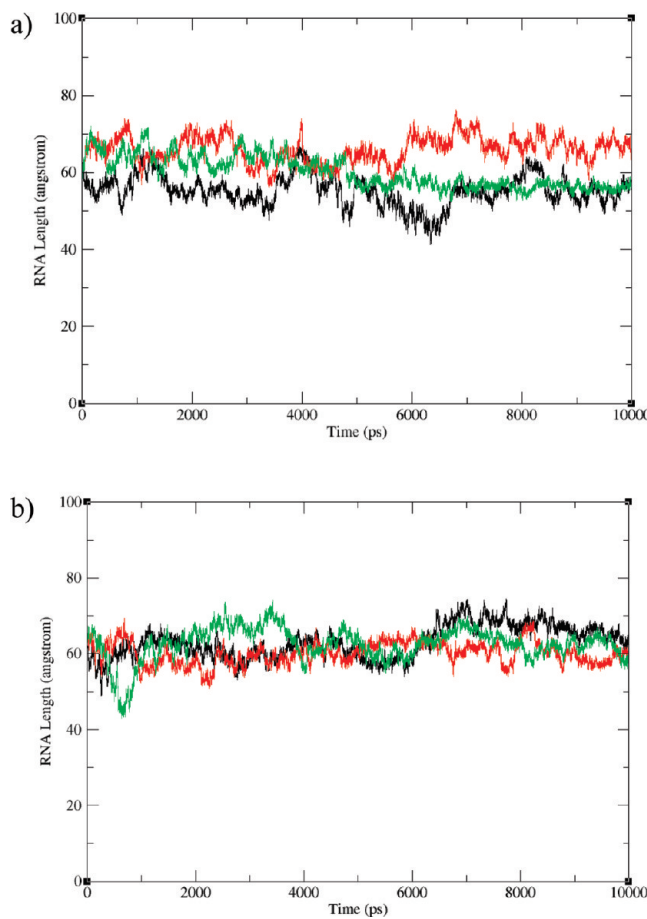


**Figure 6.** RNA length vs time of polymer–RNA complexation in 10 ns: (a) 4<sup>+</sup>G1–RNA complex and (b) 8<sup>+</sup>G1–RNA complex (0.6/1, black; 1/1, red; and 2/1, green).

was calculated with the 3DNA software,<sup>35</sup> and the error bars indicate the standard deviation associated with averaging along the length of the strand at any given time (i.e., an indication of the degree of site-specific variation in groove width along the strand). Examination of Figure 5 reveals that both the temporal and the spatial fluctuations of the major groove width are reduced in comparison with both free siRNA in water<sup>36</sup> and the single-polymer complexes examined in the companion paper (DOI: 10.1021/jp911906e), with an almost steady-state RNA major groove width of RNA in the complex at a charge ratio of 2/1. A similar trend of relatively small fluctuations in RNA length is also noted (Figure 6). It appears therefore that the increasing degree complexation of the siRNA leads to greater stabilization of the RNA structure—in the sense that spatial and temporal fluctuations are reduced. Because these are short RNA strands, we do not anticipate substantial compaction; however, it is possible that this stabilization of structure is an indicator at the short-strand limit of the kind of stabilization effects that lead to compaction for longer strands.

During the MD simulations, the carriers quickly change their starting position and bind to siRNA, as shown in Figure 1. This process can be tracked by examining the numbers of close contacts between carrier and gene as the simulation proceeds. In Figure 7, the time dependence of the number of contacts between RNA and polymer is shown for the simulations. It is quite clear that the number of contacts rises sharply during the first 1 ns of the simulation for different charge ratio. Overall, this behavior reflects a process of quick binding of RNA with the cationic polymer followed by minor adjustments to their

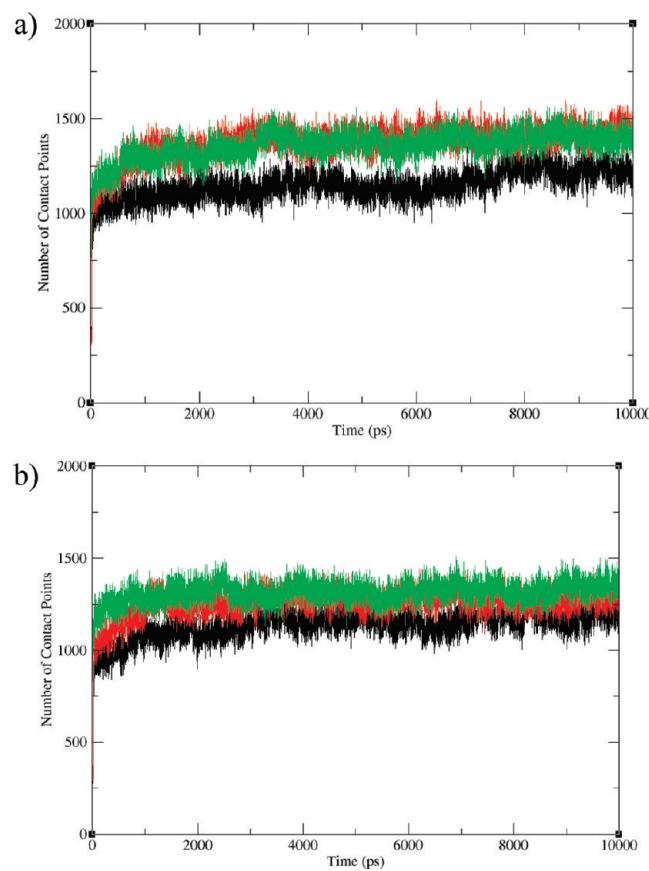


**Figure 7.** Variation of the number of contact points between polymer and RNA (any contact within 3 Å) during 10 ns simulations: (a) 4<sup>+</sup>G1–RNA complex and (b) 8<sup>+</sup>G1–RNA complex (0.6/1, black; 1/1, red; and 2/1, green).

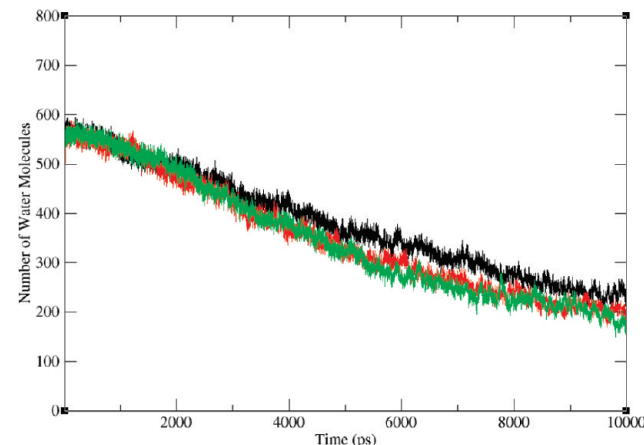


**Figure 8.** Number of water molecules in a spine of hydration (any contact within 3 Å of the siRNA) as a function of time for complexation between 4<sup>+</sup>G0 and siRNA during 10 ns simulations (0.6/1, black; 1/1, red; and 2/1, green).

configuration as final equilibration is reached. Interestingly, although the number of binding polymers (4<sup>+</sup>G0 and 8<sup>+</sup>G1) binding at a charge ratio of 2/1 are quite different, the number of contact points remains quite similar; this further confirms “electrostatic interaction” as the predominating factor to reaching equilibrium for such systems. Figure 8 shows the plot of the number of water molecules that are within 3 Å of RNA versus time. It is obvious that the number of solvating water molecules around RNA decreases significantly during the complexation process. It is mainly caused by effective displacement of hydrating water molecules by the other partner in the complex

(in this case the siRNA) since the present simulation involves relatively short RNA strands. Moreover, the number of water molecules decreases even further as the charge ratio (N/P) is raised. The general behavior observed in Figure 7 correlates qualitatively with experimental observations provided by the ethidium bromide displacement assay.<sup>37,38</sup>

#### 4. Conclusions

In conclusion, our present simulations provide a detailed molecular level understanding of both structural and dynamical aspects of multiple cationic vector–siRNA complexation. At a low charge ratio, all polymers can bind to siRNA, while only a limited number of polymers complex with the double-stranded gene at a high charge ratio. We observed reduced fluctuations in RNA structures when complexed with multiple polymers in solution as compared to both free siRNA in water and the single polymer complexes. This is the first MD simulation report for multiple polymer–siRNA complexation at different charge ratios in the literature to reflect typical ratios used in experimental transfection studies.

**Acknowledgment.** We acknowledge generous allocations of CPU time from the Australian National Computing Infrastructure (NCI) facility and the Computational Molecular Science Cluster Computing Facility at The University of Queensland, funded in part by the Australia Research Council (ARC) Linkage, Infrastructure, Equipment and Facilities (LIEF) scheme (Grant Number LE0882357).

**Supporting Information Available:** Chemical structures of four polymers (Figure S-1), snapshots of 4<sup>+</sup>linearlysine–siRNA complex at 10 ns simulation (Figure S-2), snapshots of 8<sup>+</sup>linearlysine–siRNA complex at 10 ns simulation (Figure S-3), rmsd vs time of polymer–RNA complexation in 10 ns (Figure S-4), major groove width of siRNA (averaged along the strand) vs time (Figure S-5), and RNA length vs time of polymer–RNA complexation in 10 ns (Figure S-6). This material is available free of charge via the Internet at <http://pubs.acs.org>.

#### References and Notes

- Dobson, J. *Gene Ther.* **2006**, *13*, 283.
- Park, T. G.; Jeong, J. H.; Kim, S. W. *Adv. Drug Delivery Rev.* **2006**, *58*, 467.
- Parekh, H. S. *Curr. Pharm. Des.* **2007**, *13*, 2837.
- Volcke, C.; Pirotton, S.; Grandfils, C.; Humbert, C.; Thiry, P. A.; Ydens, I.; Dubois, P.; Raes, M. *J. Biotechnol.* **2006**, *125*, 11.
- Parker, A. L.; Oupicky, D.; Dash, P. R.; Seymour, L. W. *Anal. Biochem.* **2002**, *302*, 75.
- Clamme, J. P.; Azoulay, J.; Mely, Y. *Biophys. J.* **2003**, *84*, 1960.
- Lyulin, S. V.; Darinskii, A. A.; Lyulin, A. V. *Macromolecules* **2005**, *38*, 3990.
- Lyulin, S. V.; Vattulainen, I.; Gurtovenko, A. A. *Macromolecules* **2008**, *41*, 4961.
- Farago, O.; Gronbech-Jensen, N. *Biophys. J.* **2007**, *92*, 3228.
- Farago, O.; Ewert, K.; Ahmad, A.; Evans, H. M.; Gronbech-Jensen, N.; Safinya, C. R. *Biophys. J.* **2008**, *95*, 836.
- Thyveetil, M. A.; Coveney, P. V.; Greenwell, H. C.; Suter, J. L. *J. Am. Chem. Soc.* **2008**, *130*, 12485.
- Thyveetil, M. A.; Coveney, P. V.; Greenwell, H. C.; Suter, J. L. *J. Am. Chem. Soc.* **2008**, *130*, 4742.
- Maiti, P. K.; Bagchi, B. *Nano Lett.* **2006**, *6*, 2478.
- Pavan, G. M.; Danani, A.; Prich, S.; Smith, D. K. *J. Am. Chem. Soc.* **2009**, *131*, 9686.
- Gus'kova, O. A.; Pavlov, A. S.; Khalatur, P. G.; Khokhlov, A. R. *J. Phys. Chem. B* **2007**, *111*, 8360.
- Case, D. A.; Cheatham, T. E.; Darden, T.; Gohlke, H.; Luo, R.; Merz, K. M.; Onufriev, A.; Simmerling, C.; Wang, B.; Woods, R. J. *J. Comput. Chem.* **2005**, *26*, 1668.
- Putral, L. N.; Bywater, M. J.; Gu, W.; Saunders, N. A.; Gabrielli, B. G.; Leggett, G. R.; McMullan, N. A. *Mol. Pharmacol.* **2005**, *68*, 1311.
- Case, D. A.; Darden, T. A.; Cheatham, I. T. E.; Simmerling, C. L.; Wang, J.; Duke, R. E.; Luo, R.; Merz, K. M.; Pearlman, D. A.; Crowley, M.; Walker, R. C.; Zhang, W.; Wang, B.; Hayik, S.; Roitberg, A.; Seabra, G.; Wong, K. F.; Paesani, F.; Wu, X.; Brozell, S.; Tsui, V.; Gohlke, H.; Yang, L.; Tan, C.; Mongan, J.; Hornak, V.; Cui, G.; Beroza, P.; Mathews, D. H.; Schafmeister, C.; Ross, W. S.; Kollman, P. A. *AMBER 9*; University of California: San Francisco, 2006.
- Pearlman, D. A.; Case, D. A.; Caldwell, J. W.; Ross, W. S.; Cheatham, T. E.; Debolt, S.; Ferguson, D.; Seibel, G.; Kollman, P. *Comput. Phys. Commun.* **1995**, *91*, 1.
- Wang, J. M.; Cieplak, P.; Kollman, P. A. *J. Comput. Chem.* **2000**, *21*, 1049.
- Wang, J. M.; Wolf, R. M.; Caldwell, J. W.; Kollman, P. A.; Case, D. A. *J. Comput. Chem.* **2005**, *26*, 114.
- Darden, T.; York, D.; Pedersen, L. *J. Chem. Phys.* **1993**, *98*, 10089.
- Essmann, U.; Perera, L.; Berkowitz, M. L.; Darden, T.; Lee, H.; Pedersen, L. G. *J. Chem. Phys.* **1995**, *103*, 8577.
- Crowley, M. F.; Darden, T. A.; Cheatham, T. E.; Deerfield, D. W. *J. Supercomputing* **1997**, *11*, 255.
- Sagui, C.; Darden, T. A. P3M and PME: a Comparison of the Two Methods; Workshop on Treatment of Electrostatic Interactions in Computer Simulations of Condensed Media; Amer Inst Physics: Melville, NY, 1999.
- Toukmaji, A.; Sagui, C.; Board, J.; Darden, T. *J. Chem. Phys.* **2000**, *113*, 10913.
- Sagui, C.; Pedersen, L. G.; Darden, T. A. *J. Chem. Phys.* **2004**, *120*, 73.
- Jorgensen, W. L.; Chandrasekhar, J.; Madura, J. D.; Impey, R. W.; Klein, M. L. *J. Chem. Phys.* **1983**, *79*, 926.
- Leach, A. R. *Molecular Modelling: Principles and Applications*, 2nd ed.; Prentice Hall: New York, 2001.
- Höltje, H.-D.; Sippl, W.; Rognan, D.; Folkers, G. *Molecular Modeling: Basic Principles and Applications*, 3rd ed.; Wiley-VCH: Weinheim, 2008.
- Ryckaert, J. P.; Ciccotti, G.; Berendsen, H. J. C. *J. Comput. Phys.* **1977**, *23*, 327.
- Cerutti, D. S.; Duke, R.; Freddolino, P. L.; Fan, H.; Lybrand, T. P. *J. Chem. Theory Comput.* **2008**, *4*, 1669.
- Berendsen, H. J. C.; Postma, J. P. M.; Vangunsteren, W. F.; Dinola, A.; Haak, J. R. *J. Chem. Phys.* **1984**, *81*, 3684.
- Wu, X. W.; Brooks, B. R. *Chem. Phys. Lett.* **2003**, *381*, 512.
- Lu, X. J.; Olson, W. K. *Nucleic Acids Res.* **2003**, *31*, 5108.
- Ouyang, D. F.; Zhang, H.; Herten, D. P.; Parekh, H. S.; Smith, S. C. *Aust. J. Chem.* **2009**, *62*, 1054.
- Yamagata, M.; Kawano, T.; Shiba, K.; Mori, T.; Katayama, Y.; Niidome, T. *Bioorg. Med. Chem.* **2007**, *15*, 526.
- Mannisto, M.; Vanderkerken, S.; Toncheva, V.; Elomaa, M.; Ruponen, M.; Schacht, E.; Urtti, A. *J. Controlled Release* **2002**, *83*, 169.

JP911913C